CORA Cork Open Research Archive
Cartlann Taighde Oscailte Chorcaí

Title	Femtosecond-to-second time-resolved spectroscopy brings unparalleled insight into the life cycle of the versatile manganese photocatalyst [Mn2(CO)10]
Authors	Eastwood, Jonathan B.;Rankine, Conor D.;Burden, Thomas J.;Frith, Abigail;Hammarback, L. Anders;Procacci, Barbara;Shaw, Daniel J.;O'Donoghue, Benjamin R.;Clark, Ian P.;Karas, Gabriel;Malakar, Partha;Greetham, Gregory M.;Towrie, Michael;Hunt, Neil T.;McGlacken, Gerard P.;Fairlamb, Ian J. S.;Lynam, Jason M.
Publication date	2026-04-08
Original Citation	Eastwood, J B, Rankine, C D, Burden, T J, Frith, A, Hammarback, L A, Procacci, B, Shaw, D J, O'Donoghue, B R, Clark, I P, Karas, G, Malakar, P, Greetham, G M, Towrie, M, Hunt, N T, McGlacken, G P, Fairlamb, I J S & Lynam, J M 2026, 'Femtosecond-to-second time-resolved spectroscopy brings unparalleled insight into the life cycle of the versatile manganese photocatalyst [Mn2(CO)10]', Journal of the American Chemical Society, vol. 148, no. 15, pp. 15450-15462. https://doi.org/10.1021/jacs.5c16761
Type of publication	Article (peer-reviewed)
Link to publisher's version	https://www.scopus.com/pages/publications/105036584304 - 10.1021/jacs.5c16761https://www.scopus.com/pages/publications/105036584304?origin=resultslist
Rights	© 2026, the Authors. Published by American Chemical Society. - https://creativecommons.org/licenses/by/4.0/
Download date	2026-10-30 22:28:21
Item downloaded from	https://hdl.handle.net/10468/18935



University College Cork, Ireland
Coláiste na hOllscoile Corcaigh

JACS
JOURNAL OF THE AMERICAN CHEMICAL SOCIETY
pubs.acs.org/JACS
Article

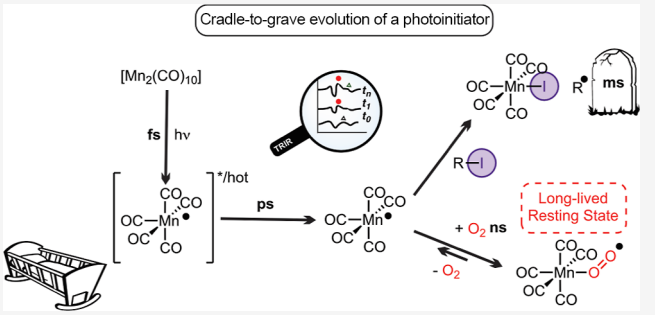
Open Access
This article is licensed under CC-BY 4.0

Femtosecond-to-Second Time-Resolved Spectroscopy Brings Unparalleled Insight Into the Life Cycle of the Versatile Manganese Photocatalyst $[Mn_2(CO)_{10}]$

Jonathan B. Eastwood, Conor D. Rankine, Thomas J. Burden, Abigail Frith, L. Anders Hammarback, Barbara Procacci, Daniel J. Shaw, Benjamin R. O'Donoghue, Ian P. Clark, Gabriel Karas, Partha Malakar, Gregory M. Greetham, Michael Towrie, Neil T. Hunt, Gerard P. McGlacken, Ian J. S. Fairlamb,* and Jason M. Lynam*

Cite This: J. Am. Chem. Soc. 2026, 148, 15450−15462
Read Online
ACCESS | Metrics & More | Article Recommendations | Supporting Information

ABSTRACT: Visible-light-activated radical photoinitiators are pivotal in the efficient construction of complex molecular architectures and the precision synthesis of advanced polymeric materials. At the heart of their function lies the formation of reactive radical species that drive selective homolytic bond cleavage, but elucidating the fundamental mechanisms of these processes is notoriously difficult due to the fleeting nature of key intermediates. In this study, time-resolved infrared (TRIR) spectroscopy provides a powerful window into the complete reaction profile of the versatile photocatalyst $[Mn_2(CO)_{10}]$, including the observation of $[Mn(O_2)(CO)_5]$, which is a long-lived (ms) reservoir of the reactive 17-electron complex $[Mn(CO)_5]$. We give unprecedented structural and mechanistic insights concerning the formation of $[Mn(CO)_5]$ in electronically and vibrationally excited states (fs−ps), its quenching by O_2 (ns), regeneration of the ground-state catalyst, and C−I bond activation (ms). New avenues for the rational design of next-generation metal−metal photocatalysts are provided, as $[Mn(O_2)(CO)_5]$ significantly extends the catalyst longevity.



INTRODUCTION

The use of light-driven reactions to promote the assembly of complex molecular frameworks is critical to modern chemical synthesis.[1−3] The key factors underpinning these breakthroughs are inorganic and organic photosensitizers that absorb visible light, resulting in the subsequent generation of reactive, open-shell, intermediates.[4,5] This can be achieved through a number of pathways; for example, the optically generated excited states of photosensitizers are simultaneously better oxidizing and reducing agents than their electronic ground states, thus enabling single-electron transfer reactions and access to doublet radicals. In addition, photosensitizers can promote energy-transfer processes which can sensitize reaction substrates to form triplet excited states, offering diverse reaction pathways when compared to their electronic ground states.[6]

An alternative method to access reactive radicals is through homolytic bond cleavage. Although this can be achieved directly through the use of either high-energy UV irradiation or thermal radical initiators, using a visible-light photoinitiator as a promoter has significant practical advantages.[7] Transition-metal-based photoinitiators are attractive as they frequently have suitable absorption bands in the visible region of the spectrum which, on excitation, can generate reactive abstractor radicals through metal−metal or metal−ligand bond cleavage (Figure 1a). These abstractor radicals can then, in turn, activate a substrate to reveal a reactive organic radical that can undergo subsequent downstream chemistry and productive bond-forming processes.

The dimeric manganese carbonyl complex $[Mn_2(CO)_{10}]$ is a leading photoinitiator and has played a significant role in the development of new transformations for synthetic chemistry and as a versatile initiator for polymer synthesis.[8−11] For example, light-activated $[Mn_2(CO)_{10}]$ promotes (1) halogen-atom transfer (XAT) reactions by the abstraction of a halogen atom from a carbon−halogen bond to enable the assembly of diverse structural motifs;[8,12−25] (2) radical polymerization processes initiated through carbon−halogen bond cleavage,[26,27] (3)

Received: September 23, 2025
Revised: March 14, 2026
Accepted: March 17, 2026
Published: April 9, 2026



Downloaded via 212.129.79.62 on May 5, 2026 at 08:47:03 (UTC).
See https://pubs.acs.org/sharingguidelines for options on how to legitimately share published articles.

ACS Publications
© 2026 The Authors. Published by American Chemical Society

https://doi.org/10.1021/jacs.5c16761
J. Am. Chem. Soc. 2026, 148, 15450−15462

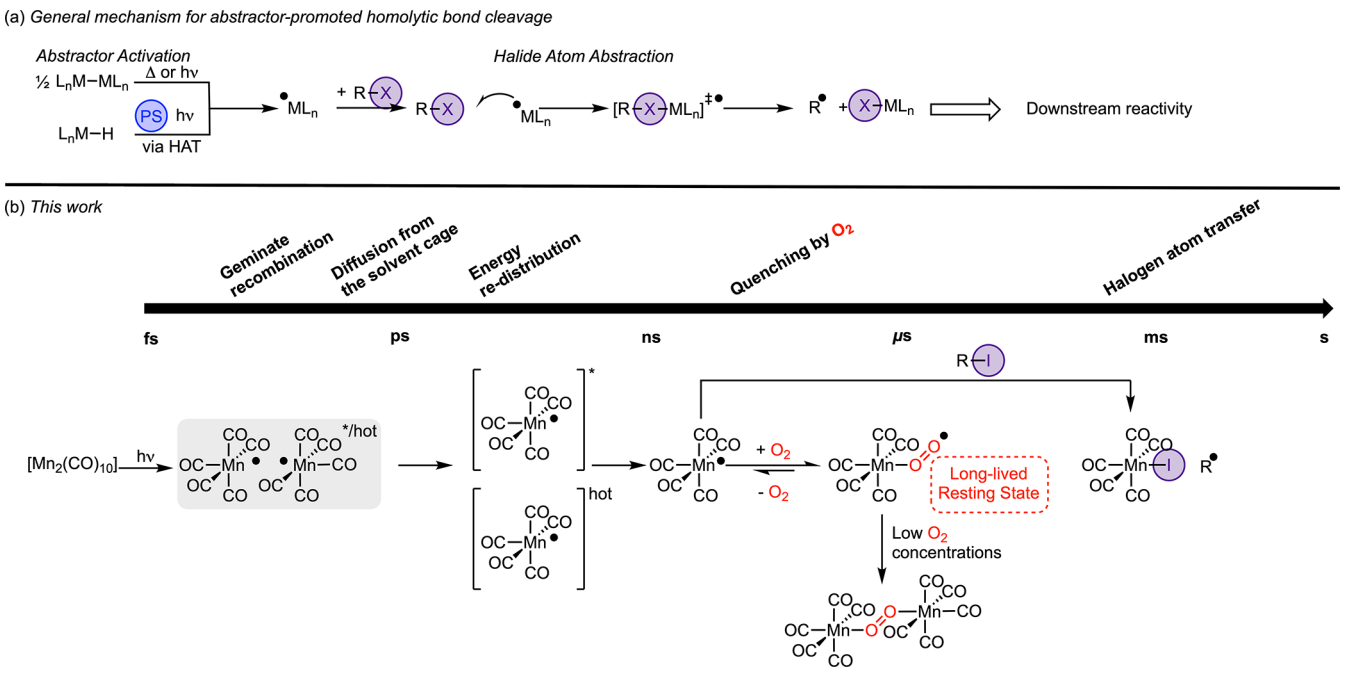


Figure 1. (a) General mechanistic steps for abstractor-initiated homolytic bond cleavage reactions using XAT as an exemplar (HAT = hydrogen-atom transfer, PC = photocatalyst). (b) Key findings from this work.

element−hydrogen bond activation to facilitate hydrosilylation and hydrogermylation,[14,28,29] (4) RAFT (reversible addition-fragmentation chain-transfer) polymerization through C−S bond activation in dithiocarbonyls,[30] and (5) N−Cl bond activation for the remote functionalization of amines.[31]

Mechanistically, it has been proposed that these reactions proceed via Mn−Mn bond cleavage to give 17-electron $[Mn(CO)_5]$ which promotes homolytic bond cleavage in the desired substrate. This is consistent with previous time-resolved spectroscopic measurements, demonstrating that $[Mn_2(CO)_{10}]$ may undergo two different light-driven processes. High-energy irradiation ($\lambda < 400$ nm) results primarily in CO dissociation to give $[Mn_2(CO)_9]$,[32] whereas the dominant pathway with lower-energy irradiation ($\lambda > 400$ nm) gives $[Mn(CO)_5]$.[33−35]

In the case of carbon−halogen bond activation, blue-light-promoted radical reactions using $[Mn_2(CO)_{10}]$ are therefore expected to give $[MnX(CO)_5]$ (X = Cl, Br, I) through homolytic R−X bond cleavage and Mn−X bond formation. This process underpins the application of the photochemical functionalization of organic molecules through XAT reactions, where an organohalide is activated by carbon−halogen bond cleavage and the resulting carbon-based radical undergoes subsequent bond-forming reactions.[7] In some cases, the initial halogen-atom transfer to manganese is thought to be followed by cyclization and then reabstraction of the halide from $[MnX(CO)_5]$, a process proposed to be driven by the stronger C−X bond dissociation energies in the product when compared to the starting material.[12,13]

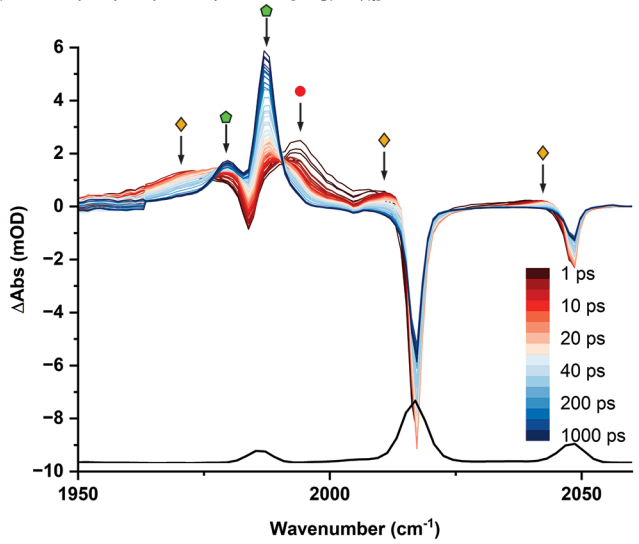
Developing a quantitative understanding of these Mn-promoted reactions is therefore important across a range of fields, especially as there is interest in the incorporation of alternative coligands into the coordination sphere of manganese, a process that enabled the development of new transformations for the hydrosulfonylation[36] and hydrofluoroalkylation of alkenes,[37] as well as CO_2 reduction.[38] A detailed mechanistic picture of these reactions would therefore enable the rational design of new metal−metal-based catalyst systems and transformations, complementing ubiquitous Ir-based photocatalyst systems. However, obtaining such information through direct observation of the key intermediates is extremely challenging, primarily due to the short lifetime of the radical species involved.

It was envisaged that the full life cycle of $[Mn(CO)_5]$ could be observed under real catalytic conditions using time-resolved spectroscopy. Using an XAT reaction as an example system, this would include (1) capturing and understanding the ultrafast dynamics of its initial light-induced generation from $[Mn_2(CO)_{10}]$, (2) providing insight into its subsequent interaction with the catalytic reaction medium, and (3) defining the ultimate role in halogen atom abstraction leading to substrate activation. Time-resolved infrared (TRIR) spectroscopy represents an ideal tool to obtain this mechanistic information as the vibrational modes of the manganese-bound carbonyl ligands are structure-sensitive probes of the metal coordination environment with high response factors. This allows the fate and dynamics of the complex to be readily determined.[39−52] Experiments were designed in which an initial laser pump pulse (400 nm) would activate $[Mn_2(CO)_{10}]$ and the subsequent formation and fate of $[Mn(CO)_5]$ could be monitored through a subsequent probe pulse in the mid-IR region to observe the changes in the Mn−C≡O vibrational modes. Performing the experiments under the exact experimental conditions for XAT reactions would then enable the processes underpinning R−X bond activation to be directly observed, providing unique and quantitative insights into the nature of the mechanistic processes underpinning XAT reactions.

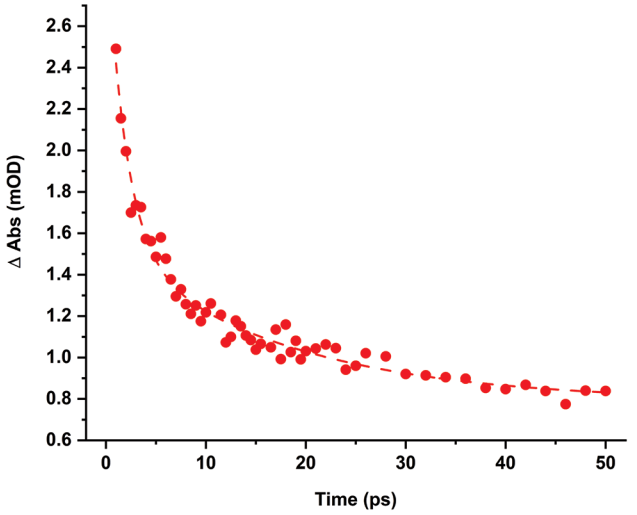
In addition, the Mn−Mn bond within $[Mn_2(CO)_{10}]$ continues to be a significant computational chemistry challenge.[53−55] As the 3*d*-valence orbitals on Mn have a limited radial extent,[56] but there is a relatively long Mn−Mn bond distance (2.895(11)—2.923(3) Å[53,57,58]—single-crystal X-ray diffraction; 2.977(11) Å—gas-phase electron diffraction[59]), there is little orbital overlap between Mn atoms. It has been proposed that there is no covalent Mn−Mn bond and that a

https://doi.org/10.1021/jacs.5c16761
J. Am. Chem. Soc. 2026, 148, 15450−15462

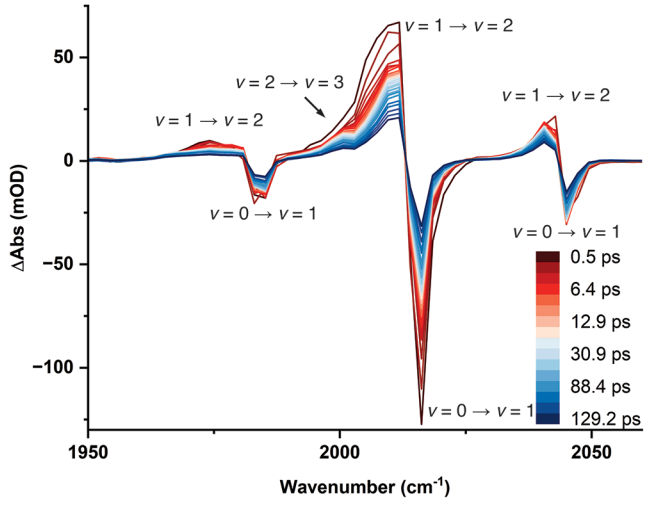
(a) 400 nm pump/IR probe spectra of $[Mn_2(CO)_{10}]$.



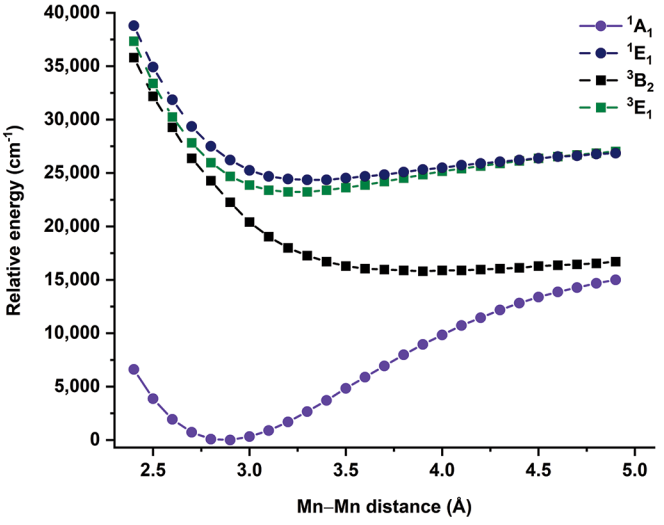
(b) Kinetic profile for the peak at 1994 cm^{-1}.



(c) IR pump/IR probe spectra of $[Mn_2(CO)_{10}]$ showing position of hot bands.



(d) Surface scan showing relative energy of the electronic states of $[Mn_2(CO)_{10}]$.



(e) Ultra-fast behavior of $[Mn_2(CO)_{10}]$.

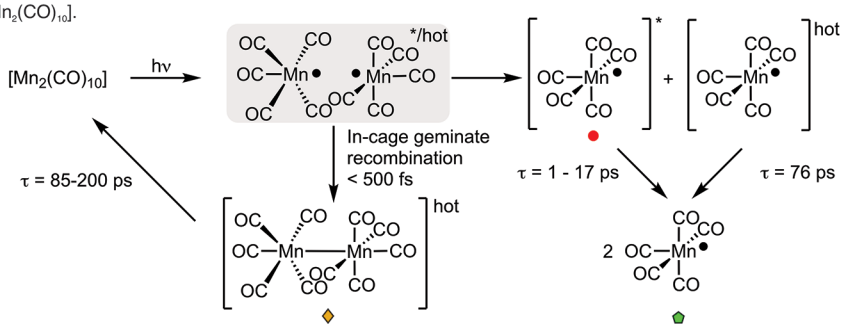


Figure 2. Ultrafast spectroscopy and calculations for the photolysis of $[Mn_2(CO)_{10}]$: (a) 400 nm pump/IR probe spectra of $[Mn_2(CO)_{10}]$ in heptane solution, with pump−probe delays between 1 ps (dark red) and 1 ns (dark blue). The black spectrum is an FTIR spectrum of $[Mn_2(CO)_{10}]$ in heptane. (b) Kinetic profile showing the temporal evolution of the peak at 1994 cm^{-1} between 1 and 50 ps. The dashed line is a fit to a biexponential function with $\tau = (1.9 \pm 0.6)$ and $(17.4 \pm 9.1$ ps) and $R^2 = 0.974$. An offset has been added to the fit to account for the overlap with the band due to $[Mn(CO)_5]$. (c) IR pump/IR probe spectrum of $[Mn_2(CO)_{10}]$ in heptane solution with pump−probe delays between 0.15 ps (dark red) and 147 ps (dark blue), showing the band position for the vibrationally excited states. (d) Surface scan showing the relative energy of the lowest lying excited states of $[Mn_2(CO)_{10}]$ as a function of Mn−Mn bond distance. Energies were determined at the CASPT2(14,14)/ANO-RCC-VDZP level of theory. (e) Summary of the ultrafast behavior of $[Mn_2(CO)_{10}]$; the colored shapes assigned to the structures refer to the assignment given in (a).

charge-shift bonding model better describes the ground-state electronic structure.[54,55] Building on the hypothesis of using charge densities to quantify the bonding within $[Mn_2(CO)_{10}]$,[53] a recent quantum crystallography study reinforces the notion that there is little electron density accumulated between the Mn atoms in the dimer.[60] Also, the recent syntheses of $[FeMn(CO)_{10}]^{+}$[61] and $[Fe_2(CO)_{10}]^{2+}$,[62] both of which are isoelectronic with $[Mn_2(CO)_{10}]$, demonstrate the wider importance of

https://doi.org/10.1021/jacs.5c16761
J. Am. Chem. Soc. 2026, 148, 15450−15462

obtaining a quantitative understanding of the structure, bonding, dynamics, and reactivity of this class of compound.

Goals of This Study

The aim of this work was to investigate XAT reactions promoted by $[Mn_2(CO)_{10}]$ using time-resolved multiple probe spectroscopy[63] (TR^MPS) on the LIFEtime spectrometer[64] at the Rutherford Appleton Laboratory. By synchronizing the pump and probe laser pulses with different repetition rates, TR^MPS was employed to record data with pump−probe delays ranging from 500 fs to 50 ms, allowing the fate of manganese over a wide temporal window to be observed. Furthermore, by integrating these measurements with time-resolved spectra using the rapid-scan IR technique, data covering a temporal range from 500 fs to minutes have been obtained, so the full life cycle of the XAT reaction can be observed (Figure 1b). The successful realization of this strategy is now reported, and unique insights into the catalytic processes underpinning the activity of $[Mn_2(CO)_{10}]$ are reported. These include the observation of a Mn-based superoxide complex, which acts as a reservoir of $[Mn(CO)_5]$, prolonging its lifetime. The outstanding spectroscopic resolution and dynamic range of the LIFEtime instrument have enabled hitherto undetected dynamics in the photochemistry of $[Mn_2(CO)_{10}]$, related to the cleavage of the Mn−Mn bond and generation of the $Mn(CO)_5$ radical to be observed. These studies demonstrate how the nature of the Mn photocatalyst is profoundly affected by the reaction conditions employed and provide a guide for future synthetic efforts.

RESULTS AND DISCUSSION

Femtosecond and Picosecond Dynamics of $[Mn_2(CO)_{10}]$ and $[Mn(CO)_5]$

To investigate the mechanistic processes underpinning $[Mn_2(CO)_{10}]$-promoted XAT reactions, a strategy was envisaged in which the complexity of the experiment was systematically increased. In the first instance, the solution-phase behavior of $[Mn_2(CO)_{10}]$ would be investigated and then experiments performed with the substrate added. This is a powerful method to observe directly key states in catalytic reactions as it enables the interactions in complex mixtures to be systematically deconvoluted.[39−41,45,46,52]

The initial studies focused on the photochemistry of $[Mn_2(CO)_{10}]$ in different solvent media by using time-resolved spectroscopy. Visible,[32,65] IR,[33] or X-ray probes[34] have been previously used to investigate the formation of $[Mn(CO)_5]$, with the aim of delineating the full details of a complex reaction in operando. However, we recognized that the significantly greater spectroscopic resolution and dynamic range of the LIFEtime spectrometer, coupled with the wide temporal range of TR^MPS, would allow for the complete evolution of the system to be obtained. This would provide a detailed cradle-to-grave map for XAT reactions and a global understanding of the factors controlling these reactions.

The photochemistry of $[Mn_2(CO)_{10}]$ was, therefore, initially investigated in solvents with varying properties. Samples were activated by a short (150 fs) laser pulse (λ = 400 nm), and the subsequent changes in the vibrational spectra between ca. 1850 and 2200 cm^{-1} were used to rationalize the nature and dynamics of the resulting photoproducts. Data are presented as difference spectra, with negative peaks indicating species lost on irradiation and positive features corresponding to the newly formed photoproducts. The spectra collected in this manner for $[Mn_2(CO)_{10}]$ in heptane are shown in Figure 2a. Three negative peaks were observed at 1983, 2014, and 2046 cm^{-1}, corresponding to the B_2-, E-, and B_2-symmetric Mn−C≡O stretching modes of $[Mn_2(CO)_{10}]$, respectively (black spectrum, Figure 2a),[66] confirming that this molecule was lost on photolysis. At pump−probe delays between 1 ps and 1 ns, several important positive features were observed, providing information about the early time dynamics of the system. At 1 ps, the major positive band in these spectra was centered at ∼1994 cm^{-1} (Figure 2a, red circle) which, over the course of 20 ps (Figure 2b), decreased in intensity, coinciding with the buildup of the signal for two bands, ∼1987 and ∼1980 cm^{-1} (Figure 2a, green pentagon). These two new features were assigned to the E- and A_1-symmetric vibrational modes of C_{4v}-symmetric[34,67] $[Mn(CO)_5]$, respectively. Although the identity of $[Mn(CO)_5]$ was secured by comparison to the literature data,[67] the species responsible for the peak at 1994 cm^{-1} has not been described previously.

The possibility of this band at 1994 cm^{-1} being due to vibrationally excited $[Mn(CO)_5]$ ($[Mn(CO)_5]^{hot}$) was excluded as the peak position is shifted to a higher frequency than the $\nu = 0 \rightarrow \nu = 1$ transition in $[Mn(CO)_5]$; the anharmonic nature of the vibrational potential energy well entails that transitions between higher vibrational energy levels are at a sequentially lower energy. Furthermore, the possibility that the change in band position from 1994 cm^{-1} to 1987 and 1980 cm^{-1} was due to intramolecular vibration redistribution of $[Mn(CO)_5]$ was also excluded, as this would again result in a shift in band position to a higher, rather than lower, energy.[68]

Several other assignments were considered. The possibility of the band being due to vibrationally excited $[Mn_2(CO)_{10}]$ was investigated by using an IR pump/IR probe experiment using a spectrometer system in York. There, a 90 fs IR pump pulse excites the sample to a higher vibrational energy level, and the probe pulse then interrogates the nature of the $\nu = n \rightarrow \nu = n + 1$ transitions. The resulting spectrum (Figure 2c) allowed for the identification of the peak positions of the $\nu = 1 \rightarrow \nu = 2$ and $\nu = 2 \rightarrow \nu = 3$ transitions for $[Mn_2(CO)_{10}]$ (see Figure S19 for deconvolution).[69] This revealed anharmonicity values of 10, 6, and 4 cm^{-1} for the B_2, E, and B_2 fundamental modes of $[Mn_2(CO)_{10}]$, respectively.

Inspection of the 400 nm pump/IR probe data revealed that these spectroscopic features were also present (Figure 2a, yellow diamonds), confirming that $[Mn_2(CO)_{10}]^{hot}$ had been formed in the experiment. The peaks for $[Mn_2(CO)_{10}]^{hot}$ arise from the fact that the energy of the excitation photon is greater than the Mn−Mn bond dissociation energy, and therefore any $[Mn_2(CO)_{10}]$ reformed by the geminate recombination of $[Mn(CO)_5]$ will be in a higher vibrational energy level.[70] These peaks decreased in intensity over ca. 200 ps with a commensurate recovery of the ground-state bleach bands: an observation again consistent with the intermolecular vibrational energy transfer to the bath. In the 400 nm pump/IR probe spectra, the lifetime for the recovery of the E-symmetric bleach band was (111 ± 18) ps, whereas from the IR pump/IR probe spectra, it has been shown to be (165 ± 2) ps.[69] It is proposed that on the sub-ns timescale, the recovery of $[Mn_2(CO)_{10}]$ is solely due to vibrational relaxation and that the small discrepancy in lifetimes between the methods is due to different vibrational excited-state populations being generated between the two experiments.[71,72] Therefore, geminate recombination of two $[Mn(CO)_5]$ radicals to form $[Mn_2(CO)_{10}]^{hot}$ is faster than the 500 fs resolution of this experiment, and no recombination of $[Mn(CO)_5]$ occurs between 500 fs and 1 ns. Crucially, the

https://doi.org/10.1021/jacs.5c16761
J. Am. Chem. Soc. 2026, 148, 15450−15462

band at 1994 cm^{-1} was not present in the IR pump/IR probe experiments and, therefore, cannot be assigned to $[Mn_2(CO)_{10}]^{hot}$.

The ground-state IR spectra of $[Mn_2(CO)_{10}]$ in heptane were found to be temperature-independent over a range of 25−80 °C, excluding the possibility of a local heating effect altering the ground-state bleach position. Experiments were performed on different batches of $[Mn_2(CO)_{10}]$ from different suppliers, and identical data were obtained in all cases, excluding the possibility that the peak at 1994 cm^{-1} was due to an impurity. In addition, the dynamics were unaffected by recording the experiments at different laser pump power levels. The possibility of a heteronuclear bond cleavage occurring first to give $[Mn(CO)_5]^+[Mn(CO)_5]^-$, prior to a single-electron transfer to give two $[Mn(CO)_5]$ molecules (which may be viewed as the resonance extreme of the charge-shift bonding model),[55] was also excluded as the peak at 1994 cm^{-1} did not correspond to the reported band positions for neither $[Mn(CO)_5]^+$[73] nor $[Mn(CO)_5]^-$.[74,75] In addition, this peak cannot be due to $[Mn_2(CO)_9]$ (which is formed as a minor photoproduct at this excitation wavelength) as some of the characteristic peaks for this species (bands expected at 1975, 1997, 2016, 2039, and 2054 cm^{-1}) were absent.[76,77]

The lifetime of the peak at 1994 cm^{-1} shows a small dependence on the nature of the solvent (see Supporting Information), but the data did not show a relationship between this lifetime and solvent viscosity, which previous works by Tyler[78−82] on $[Mo(\eta^5\text{-}C_5H_4Me)(CO)_3]$ have shown, dictates the rate of radical release from a solvent cage. Hence, it was concluded that the peak at 1994 cm^{-1} was not due to two molecules of $[Mn(CO)_5]$ held within a solvent cage.

A consideration of the energetic landscape following the photodissociation of $[Mn_2(CO)_{10}]$ provides insight into the assignment of this species responsible for the band at 1994 cm^{-1}. Working in common units of cm^{-1}, the Mn−Mn bond dissociation energy is reported to be between 8000 and 14,550 cm^{-1},[55,83−89] which means, after 25,000 cm^{-1} (ca. λ = 400 nm) excitation and Mn−Mn bond cleavage, there is an excess energy between 17,000 and 10,450 cm^{-1}. Some of this is manifested in $[Mn(CO)_5]$ being formed in the vibrational excited states. However, $[Mn(CO)_5]$ exhibits a low-energy absorbance at (ca. 810 nm),[32] so it must possess electronic excited states with energies <12,346 cm^{-1}. Consequently, the peak at 1994 cm^{-1} is assigned to $[Mn(CO)]_5$ in an electronic excited state, $[Mn(CO)_5]^*$. The related generation of a photoproduct in an electronic excited state has also been reported for the following S−H bond dissociation in thiophenols.[90−92]

Over the course of ca. 200 ps, the bands for solvated $[Mn(CO)_5]$ were observed to sharpen and were fitted to a Gaussian line shape, and the full-width half-height line width plotted against time. This demonstrated a monoexponential function with a lifetime, τ, of 76 ps. This change in line shape was attributed to intermolecular vibrational energy transfer from the vibrationally excited $[Mn(CO)_5]$ ($[Mn(CO)_5]^{hot}$) to the solvent bath, commensurate with previous ps studies.[33]

To explore the behavior of the complex as the Mn−Mn bond was broken, the nature of the excited states of $[Mn_2(CO)_{10}]$, and their dependence on the Mn−Mn bond distance, was explored (Figure 2e). To model the multireference nature of the Mn−Mn bond dissociation event, the energies of the states were calculated at the CASPT2(14,14)/ANO-RCC-VDZP level of theory using an active space comprising the Mn−Mn σ-bonding and σ^*antibonding orbitals, two $3d_\delta$ orbitals, three $3d_\pi$ orbitals, and six π^*CO orbitals (see Supporting Information for details). The calculations demonstrated that the $^1A_1$ ground state had a minimum energy at a Mn−Mn bond distance of ca. 2.9 Å, consistent with experimental data.[53,57−59] The behavior of the four excited states was also explored. The lowest lying singlet excited state was found to be an optically bright $^1E_1$ state, with the σ^*(Mn−Mn) ← $3d_{\pi 2}$ character. The corresponding triplet state, $^3E_1$, was found to be almost isoenergetic at all Mn−Mn bond distances which, when taken with their spin−orbit coupling constant (calculated to be between 99 and 106 cm^{-1}, depending on the Mn−Mn distance), would imply that there is rapid intersystem crossing between the two E_1 states. Importantly, both E_1 states had a local minimum with an Mn−Mn bond distance of ca. 3.3 Å, slightly longer than the ground state but demonstrating that they are nondissociative with respect to the Mn−Mn reaction coordinate. In contrast, the lowest lying triplet state, $^3B_2$, which has σ^*(Mn−Mn) ← σ(Mn−Mn) character, is dissociative along the Mn−Mn coordinate at all bond distances examined, which when populated would result in the generation of two discrete $[Mn(CO)_5]$ molecules.

The CASPT2(14,14)/ANO-RCC-VDZP calculations also gave insight into the nature of the proposed electronic excited state $[Mn(CO)_5]^*$. Exploration of the first electronically excited (1^2E)-state potential energy surface revealed that the Franck−Condon point for $[Mn(CO)_5]$ lies at 11,050 cm^{-1} relative to the ground-state (1^2A_1) minimum-energy geometry. However, the 1^2E potential energy surface in the region of the C_{4v}-symmetric Franck−Condon geometry descends extremely steeply toward the $1^2B_1/1^2A_1$ crossing seam, characterized by C_{2v} or D_{3h} symmetry (Figure S25). This situation is reminiscent of the states formed in the photodissociation of a CO ligand from $Cr(CO)_6$,[93] in that the D_{3h} geometry is Jahn−Teller-unstable and sits at a conical intersection. The pathway between the C_{4v}-symmetric 1^2A_1 minimum-energy geometry and $1^2B_1/1^2A_1$ crossing seam on the 1^2A_1 potential energy surface is very shallow: the $1^2B_1/1^2A_1$ minimum-energy crossing point is low-lying, being located at only 3910 cm^{-1} with respect to the 1^2A_1 minimum-energy geometry.

It is therefore proposed that, following Mn−Mn bond cleavage, the excess internal energy (between 17,000 and 10,450 cm^{-1}) in the $[Mn(CO)_5]$ fragments is sufficient for the complex to explore both the ground (1^2A_1) and low-lying excited-state (1^2E) potential energy surfaces via a pseudorotation-type mechanism that facilitates interconversion between the C_{4v} and C_{2v}/D_{3h} symmetries and, consequently, the 1^2A_1 and 1^2B_1 electronic states. When this excess energy is dissipated, this is no longer possible, hence the disappearance of the peak at 1994 cm^{-1}. At the CASSCF/ANO-RCC-VDZP level, the C_{4v} ground state of $[Mn(CO)_5]$ is predicted to have MnC≡O bands at 2250 (E) and 2222 (A_1) cm^{-1}, whereas the corresponding stretches for the C_{2v} state in proximity to the $1^2B_1/1^2A_1$ crossing seam are at 2282 (A_1), 2222 (B_2), and 2197 (B_1) cm^{-1}. This indicates that the spectrum of the C_{2v}/D_{3h}-symmetric structure(s) should exhibit a peak at higher energy, consistent with the experimental observation of a band at 1994 cm^{-1}.

A summary of all the ultrafast behaviors of light-activated $[Mn_2(CO)_{10}]$ is shown in Figure 2e. The early time dynamics of $[Mn(CO)_5]$ is now fully established.

https://doi.org/10.1021/jacs.5c16761
J. Am. Chem. Soc. 2026, 148, 15450−15462

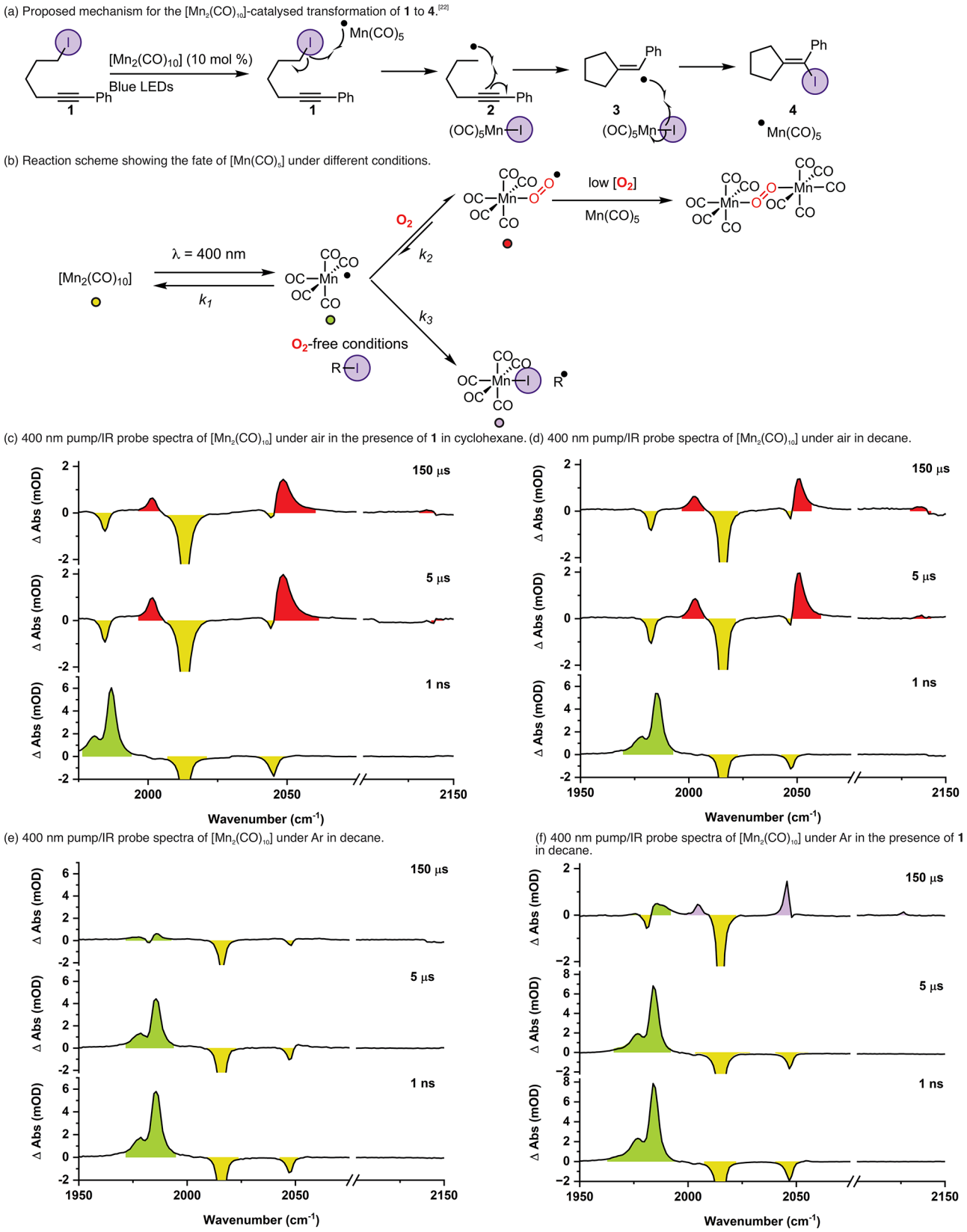


Figure 3. Spectroscopic and computational data for the interaction between light-generated $[Mn(CO)_5]$ and O_2 on ns–μs timescale. (a) Reaction scheme showing the proposed mechanism for the $[Mn_2(CO)_{10}]$-catalyzed conversion of **1** to **4**. (b) Summary of the key mechanistic findings from this work; the colored markers assigned to the compounds are consistent with the shading of the transient absorbance bands in the subsequent spectra. (c) 400 nm pump/IR probe spectra for a cyclohexane solution of $[Mn_2(CO)_{10}]$ and **1** under an air atmosphere. (d) 400 nm pump/IR probe spectra for a decane solution of $[Mn_2(CO)_{10}]$ under an air atmosphere. (e) 400 nm pump/IR probe spectra for a decane solution of $[Mn_2(CO)_{10}]$ under an Ar atmosphere. (f) 400 nm pump/IR probe spectra for a decane solution of $[Mn_2(CO)_{10}]$ and **1** under an Ar atmosphere. Bands for $[Mn_2(CO)_{10}]$ are colored in yellow, $[Mn(CO)_5]$ in green, $[Mn(O_2)(CO)_5]$ in red, and $[MnI(CO)_5]$ in purple.

https://doi.org/10.1021/jacs.5c16761
J. Am. Chem. Soc. 2026, 148, 15450−15462

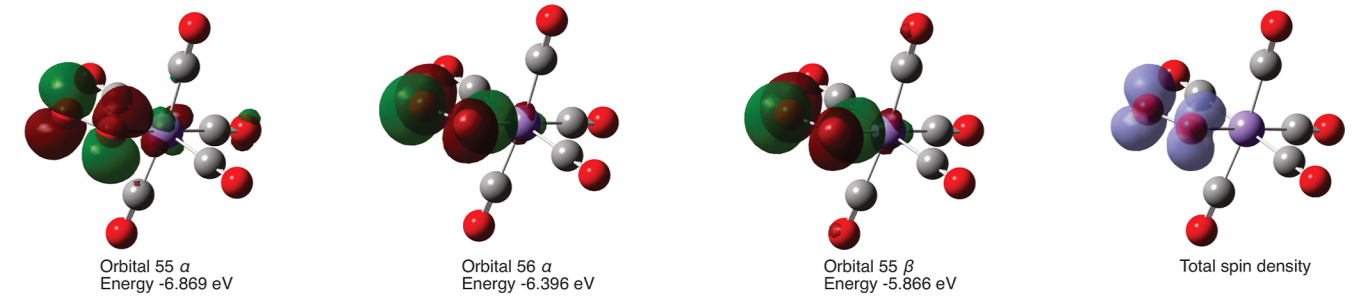


Figure 4. Two highest energy α-spin, the highest energy β-spin orbitals, and total spin density for $[Mn(O_2)(CO)_5]$ at the UPBE0/def2-TZVPP level of theory.

Nanosecond and Microsecond Observations of the Fate of $[Mn(CO)_5]$

Our next stage was to observe the key states involved in a Mn-promoted XAT reaction, and the radical cyclization reaction shown in Figure 3a was selected.[23] In this reaction, it is proposed that the iodide abstraction from **1** by $[Mn(CO)_5]$ results in the formation of $[MnI(CO)_5]$ and an alkyne radical, **2**, which then undergoes cyclization to give **3** (Figure 3a). In the initial publication, it was proposed that a rebound reaction occurs between **3** and $[MnI(CO)_5]$ to give **4**, regenerating $[Mn(CO)_5]$.[23] Interestingly, and of key importance to the findings in this work, the reaction functioned effectively under an air atmosphere with a yield similar to that obtained for a reaction under an N_2 atmosphere.

The interaction of light-generated $[Mn(CO)_5]$ with excess **1** was explored. To mimic the experimental synthetic conditions, cyclohexane was used as a solvent, and the experiments were performed under air.[23] In some experiments, 1,4-diiodobutane was selected as a second, simpler reference substrate, and/or decane was used as a solvent. The early time (fs/ps) dynamics of the solutions containing **1** were unchanged from an experiment in cyclohexane alone. They were also essentially the same as in heptane (see earlier); however, over the course of ca. 1 μs, the band for $[Mn(CO)_5]$ decreased in intensity to be replaced by three new bands at 2001, 2049, and 2136 cm^{-1}, whose relative intensity and band positions are consistent with the $A_1^{(1)}$, E, and $A_1^{(2)}$ vibrational modes of a neutral C_{4v}-symmetric complex of general formula $[MnX(CO)_5]$ (Figure 3c).[93−95] However, these peaks do not correspond to the band positions for authentic $[MnI(CO)_5]$ (the expected product for iodide abstraction), and essentially identical observations were made when **1** was omitted from the experiment (Figure 3d), demonstrating that this new species was not formed by iodine atom abstraction. It was postulated that in the presence of air, $[Mn(CO)_5]$ could undergo a nanosecond reaction with molecular oxygen to give $[Mn(O_2)(CO)_5]$. This species has previously been proposed on the basis of EPR studies[96−98] and is speculated to be an intermediate in the recently reported bromination of alkenes[16] and the functionalization of quinones.[99]

Consistent with the proposed formulation of $[Mn(O_2)(CO)_5]$, an experiment performed under an O_2 atmosphere[100] resulted in the same spectroscopic features being present as under air, but the observed rate constant for their formation from $[Mn(CO)_5]$ was a factor of 4 faster. Based on the mole fraction solubility for O_2 in cyclohexane,[101] the second-order rate constant for the reaction between $[Mn(CO)_5]$ and O_2 was calculated to be $(3.29 \pm 0.58) \times 10^9$ mol^{-1} dm^3 s^{-1}. Furthermore, experiments performed in a deoxygenated cyclohexane or decane solution of $[Mn_2(CO)_{10}]$ under argon demonstrated that only trace amounts of $[Mn(O_2)(CO)_5]$ were formed, and the dominant process, occurring over ca. 150 μs, was the recombination of two molecules of $[Mn(CO)_5]$ to reform $[Mn_2(CO)_{10}]$ (Figure 3e). In these experiments, $[Mn(O_2)(CO)_5]$ underwent a further reaction on a slower timescale to give a species with bands at 1997 and 2057 cm^{-1}. Under these oxygen-limited conditions, it is proposed that the monoradical $[Mn(O_2)(CO)_5]$ undergoes a further reaction with excess $[Mn(CO)_5]$ to give $[\{Mn(CO)_5\}_2(\mu\text{-}O_2)]$.

A series of calculations were performed to understand the electronic structure of $[Mn(O_2)(CO)_5]$. A range of different methods were employed (see Supporting Information for details), but in all cases, the optimized geometry was a square-based pyramidal $[Mn(CO)_5]$ group with an η^1-bound O_2 fragment (Figure 4). The three highest-energy α- and β-spin orbitals are shown in Figure 4, all of which may be viewed as having a π^* character localized on the O_2 ligand. Previous EPR studies on $[Mn(O_2)(CO)_5]$ have shown that hyperfine coupling between the unpaired electron density and Mn nucleus is small,[96] consistent with this computational picture. We suggest that $[Mn(O_2)(CO)_5]$ is best treated as a Mn(I) complex of a superoxide radical anion $[O_2^{\cdot-}]$, formed through the formal one-electron reduction of O_2 by $[Mn(CO)_5]$. This picture is also supported by the similarity in the experimental and DFT-predicted (unscaled BP86/SV(P)) IR spectra for $[MnI(CO)_5]$ (experimental: 2004, 2045, and 2126 cm^{-1}; predicted: 2035, 2057, and 2135 cm^{-1}) and $[Mn(O_2)(CO)_5]$ (experimental: 2001, 2049, and 2136 cm^{-1}; predicted: 2029, 2042, 2047, 2063, and 2124 cm^{-1}). The additional bands in the predicted spectrum of $[Mn(O_2)(CO)_5]$ represent the deviation from the idealized C_{4v}-symmetry in the calculated (static) structure.

Under an atmosphere of air (again mimicking the synthetic reaction conditions), little or no evidence for iodide abstraction from **1** was obtained on these timescales. However, photolysis of a solution of $[Mn_2(CO)_{10}]$ and **1** in cyclohexane, which had been exhaustively deoxygenated by sparging with argon for >10 min, resulted in $[Mn(CO)_5]$ loss and formation of $[MnI(CO)_5]$ over 100 μs (Figure 3f), consistent with a model in which $[Mn(CO)_5]$ has two competing fates, either iodide abstraction to give $[MnI(CO)_5]$ or dimerization to reform $[Mn_2(CO)_{10}]$. Kinetic modeling (see Supporting Information for details) demonstrated that the rate constant of iodide abstraction from [**1**] by $[Mn(CO)_5]$ was $(1.75 \pm 0.30) \times 10^5$ mol^{-1} dm^3 s^{-1}. The dimerization of $[Mn(CO)_5]$ to give $[Mn_2(CO)_{10}]$ was shown to have a rate constant of $(1.07 \pm 0.10) \times 10^9$ mol^{-1} dm^3 s^{-1}, the latter being consistent with previous reports.[102]

https://doi.org/10.1021/jacs.5c16761
J. Am. Chem. Soc. 2026, 148, 15450−15462

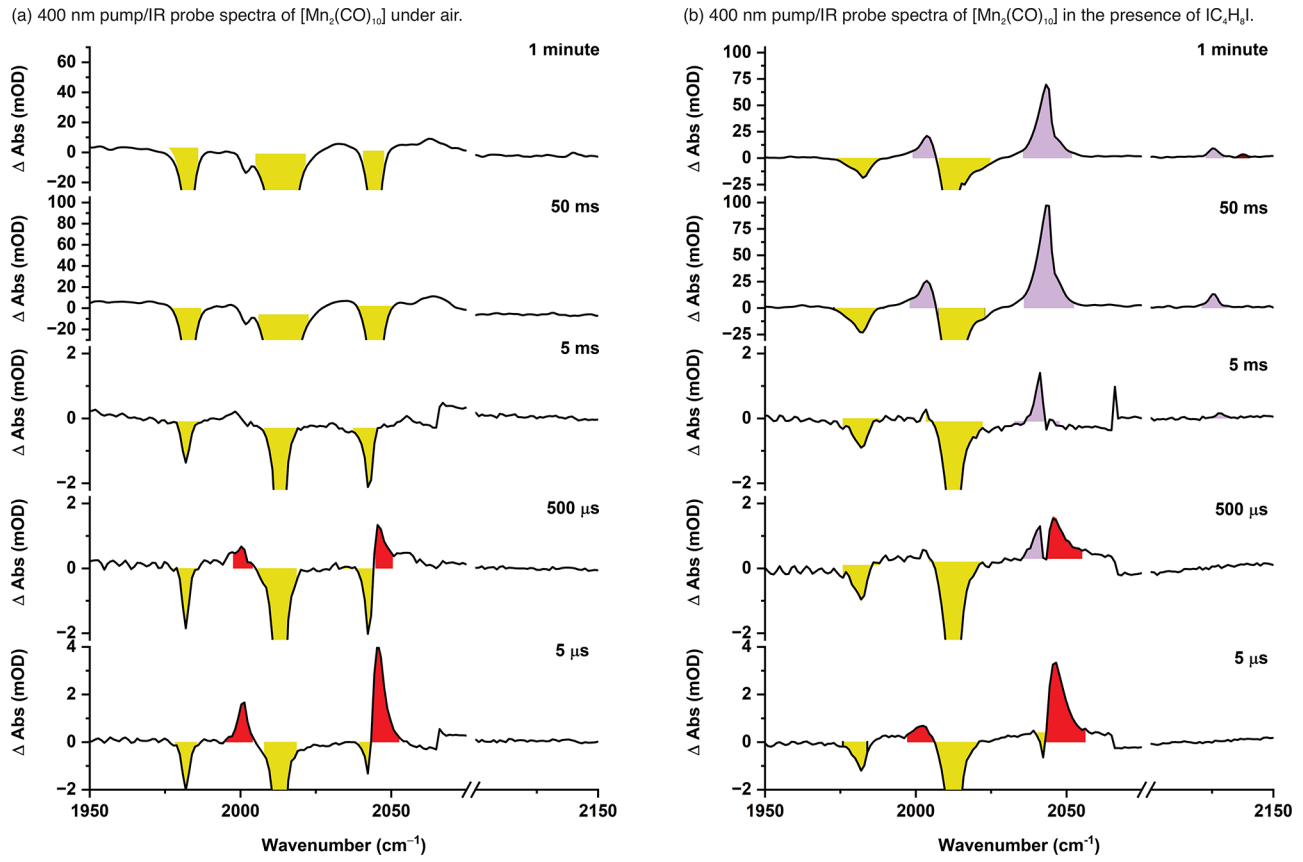


Figure 5. (a) 400 nm pump/IR probe spectra for a cyclohexane solution of $[Mn_2(CO)_{10}]$ under an air atmosphere. (b) 400 nm pump/IR probe spectra for a cyclohexane solution of $[Mn_2(CO)_{10}]$ and $I(CH_2)_4I$ under an air atmosphere. Bands for $[Mn_2(CO)_{10}]$ are colored in yellow, $[Mn(O_2)(CO)_5]$ in red, and $[MnI(CO)_5]$ in purple. Spectra with a pump−probe delay of 5 μs, 500 μs, and 5 ms were acquired on the LIFEtime instrument with a probe repetition rate of 20 Hz. Spectra with a pump−probe delay of 50 ms and 1 min were acquired on a Bruker Vertex 80 instrument in Rapid Scan mode using 405 nm LED irradiation.

These experiments also demonstrated the extreme sensitivity of these systems to molecular oxygen. For example, in several instances, the repeated data acquisitions which are normally averaged as part of the experiment had a different composition, with the first run showing clean conversion to $[MnI(CO)_5]$, but later runs forming both $[MnI(CO)_5]$ and $[Mn(O_2)(CO)_5]$, or $[Mn(O_2)(CO)_5]$ alone, presumably due to trace air entering the experimental system. Furthermore, deliberate leaking of air into a sample that had solely formed $[MnI(CO)_5]$ during its data acquisition and reacquiring the experiment resulted in the sole formation of $[Mn(O_2)(CO)_5]$.

These data challenge the canonical view of XAT reactions as they unambiguously demonstrate that under air (and even trace amounts of O_2), the primary kinetic fate of the $[Mn(CO)_5]$ radical is not halide abstraction but formation of $[Mn(O_2)(CO)_5]$. A summary of these findings is shown in Figure 3b.

Millisecond-to-Second Observation of the Key States in Photoinitiated C−X Bond Cleavage by $[Mn(CO)_5]$

The μs timescale data indicated that $[Mn(CO)_5]$ reacts rapidly with O_2 to give $[Mn(O_2)(CO)_5]$. Therefore, a key question remained: Under the synthetic reactions performed in air, how does C−I bond activation occur? To resolve the apparent dichotomy regarding the dominant formation of $[Mn(O_2)(CO)_5]$ under the catalytic reaction conditions, the acquisition protocol for the TR^{M}PS experiment was altered so that the pump pulse had a repetition rate of 20 Hz instead of 1 kHz while maintaining a 100 kHz probe repetition rate. This enabled measurements on light-activated $[Mn_2(CO)_{10}]$ using TR^{M}PS on timescales up to 50 ms, with data acquired every 10 μs. Cyclohexane solutions of $[Mn_2(CO)_{10}]$ under air were investigated in both the absence (Figure 5a) and presence (Figure 5b) of 1,4-diiodobutane as a model substrate for iodide abstraction.

In the absence of substrates, the spectra showed the formation of $[Mn(O_2)(CO)_5]$ as expected, but over the course of 2 ms, the peaks decreased in intensity. Some evidence for the negative bands for $[Mn_2(CO)_{10}]$, also decreasing in intensity, was obtained, albeit over a slightly longer timescale. However, negative bands for $[Mn_2(CO)_{10}]$ remained at longer times. When taken with the observation of small bands at 1998, 2030, and 2055 cm^{-1}, this may represent the formation of a small amount of $[Mn_2(CO)_9]$ by competitive CO loss, rather than Mn−Mn bond cleavage.[76,77,103,104] Alternatively, it is possible that $[Mn(O_2)(CO)_5]$ is unstable and may be undergoing decomposition.

Repeating the experiment in the presence of 1,4-diiodobutane showed the initial formation of $[Mn(O_2)(CO)_5]$. However, in this case, a smooth conversion to $[MnI(CO)_5]$ was observed (Figure 5b). The loss of $[Mn(O_2)(CO)_5]$ and the growth of $[MnI(CO)_5]$ were successfully fitted to first-order kinetics with statistically identical rate constants. Repeating the experiment at double the concentration of 1,4-diiodobutane resulted in essentially identical data being obtained. Again, the observed rate constants in both experiments were statistically identical.

https://doi.org/10.1021/jacs.5c16761
J. Am. Chem. Soc. 2026, 148, 15450−15462

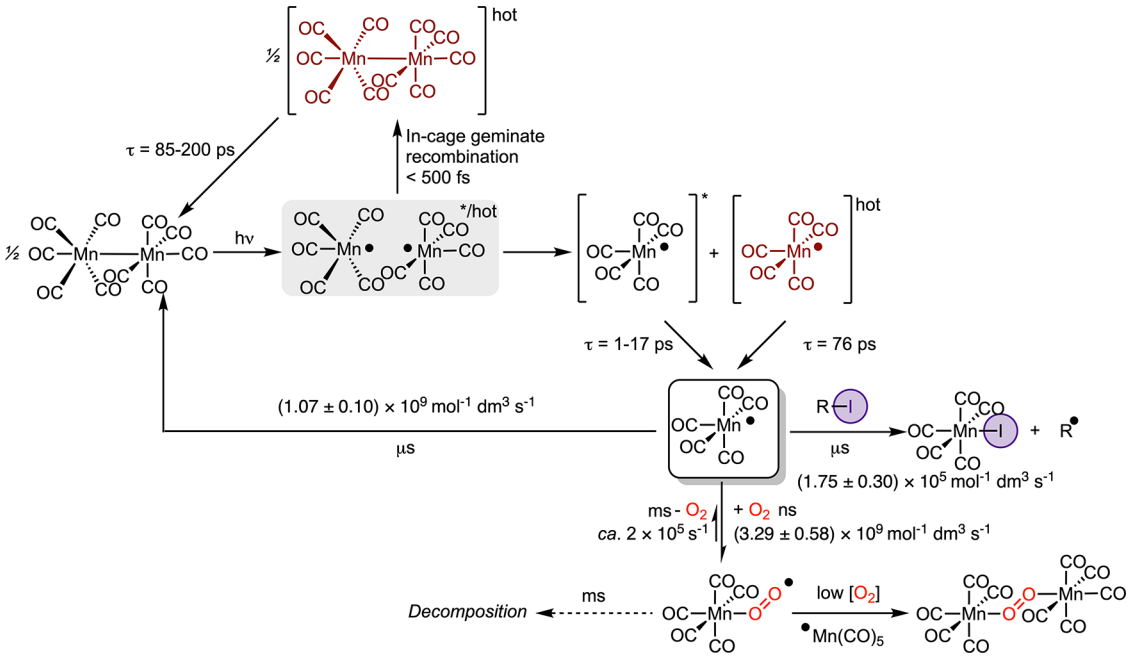


Figure 6. Global mechanism for R−I bond activation by $[Mn(CO)_5]$. The timescales given for a given process are representative of the concentration regimes used in this work.

Kinetic modeling of these data (see Supporting Information) demonstrated that $[Mn(O_2)(CO)_5]$ and $[Mn(CO)_5]$ and O_2 are in equilibrium. The loss of O_2 from $[Mn(O_2)(CO)_5]$ has a first-order rate constant of ca. 2×10^5 s^{-1}, and $[Mn(CO)_5]$ thus generated may then undergo a competitive reaction with O_2 to regenerate $[Mn(O_2)(CO)_5]$, with 1,4-diiodobutane to produce $[MnI(CO)_5]$, or dimerize to regenerate $[Mn_2(CO)_{10}]$. However, in the presence of 1,4-diiodobutane, the latter process is only a minor pathway.

Experiments were performed to study the behavior of the system on longer timescales (50 ms−min) using Rapid Scan FT-IR spectroscopy. At the earliest times investigated (50 ms), these experiments mirrored those from the TR^MPS data on LIFEtime, demonstrating the selective formation of $[MnI(CO)_5]$ when the experiment was performed in the presence of 1,4-diiodobutane and a spectrum with a low intensity in its absence.

These data therefore indicate that $[Mn(O_2)(CO)_5]$ can undergo reactions with iodine-containing substrates to give $[MnI(CO)_5]$. A mechanistic picture in which there is an equilibrium between $[Mn(O_2)(CO)_5]$ and $[Mn(CO)_5]$/molecular oxygen is consistent with these data. As no $[Mn(CO)_5]$ is observed after ca. 0.5 ms, the spectroscopic data indicate that the equilibrium lies on the side of $[Mn(O_2)(CO)_5]$. However, the subsequent reactivity (reformation of $[Mn_2(CO)_{10}]$ and iodide abstraction) illustrates that a small concentration of reactive $[Mn(CO)_5]$ is present. Strictly speaking, an alternative pathway in which $[Mn(O_2)(CO)_5]$ undergoes either a direct or indirect reaction with the alkyl iodide (i.e., not through the reversible formation of $Mn(CO)_5$) cannot be excluded on the basis of these data,[105] in particular given that the superoxide complex undergoes an apparent decomposition in the absence of a substrate.

Conclusions: A Global Mechanism for XAT by Light-Activated $[Mn_2(CO)_{10}]$

The results from this study have facilitated the deduction of the complete life cycle of a Mn carbonyl complex during an XAT reaction for the first time. This includes the fs−ps formation of the $[Mn(CO)_5]$ radical and relaxation from its vibrationally and electronically excited states; its subsequent reaction with O_2 to give $[Mn(O_2)(CO)_5]$ on a ns−μs timescale, followed by a much slower (ms) halide abstraction reaction to give $[MnI(CO)_5]$. These are summarized in Figure 6, along with all of the rate constants determined for the uni- and bimolecular processes identified in this work. One of the major findings of this work is that, unless there is rigorous exclusion of molecular oxygen from a reaction mixture (i.e., use of a dry/glovebox), $[Mn(O_2)(CO)_5]$ acts as the photocatalyst resting state, and this is important for the practicing synthetic chemist. Indeed, this may impart favorable outcomes on a given reaction, as $[Mn(CO)_5]$ undergoes recombination to give $[Mn_2(CO)_{10}]$ close to the diffusion-controlled limit. Instead, $[Mn(O_2)(CO)_5]$ acts as a relatively long-lived (ms) store of $[Mn(CO)_5]$ and is reminiscent of how N_2 and THF coordination stabilizes the highly reactive "$Cr(CO)_5$" fragment through the formation of $[Cr(CO)_5(N_2)]$[106] and $[Cr(CO)_5(THF)]$,[107] respectively. This notion is reinforced in a recent report which demonstrated that the performance of light-activated $[Mn_2(CO)_{10}]$ in a hydrosilylation reaction was found to be identically well under an atmosphere of either air, O_2, or Ar.[29]

In the case of $[Mn(O_2)(CO)_5]$, it is proposed that the reactive $[Mn(CO)_5]$ is leached into the solution at low concentrations, which limits unproductive dimerization but enables the desired halide abstraction reactions. It is therefore proposed that in some circumstances photoinitiated radical reactions may be actively promoted by molecular oxygen, and such conditions should be routinely interrogated in synthetic reaction screening protocols. The formation and decay of $[Mn(O_2)(CO)_5]$ have implications for other photochemical reactions of $[Mn_2(CO)_{10}]$ and other sources of $[Mn(CO)_5]$. Moreover, the global findings highlight the potential of metal−metal-based systems as potential photocatalysts in the future,[7] as well as illustrating how the elucidation of the reaction mechanism by time-resolved spectroscopy can highlight the unexpected role of trace reaction components. Future studies will focus on understanding the role

https://doi.org/10.1021/jacs.5c16761
J. Am. Chem. Soc. 2026, 148, 15450−15462

of the superoxide complexes in XAT reactions and will include an exploration of the role of the structure of the metalloradicals and the effects of O_2 concentration on the reaction outcomes.

■ ASSOCIATED CONTENT

Supporting Information

The Supporting Information is available free of charge at https://pubs.acs.org/doi/10.1021/jacs.5c16761.

Details of the time-resolved spectroscopy experiment, data collection and processing, synthetic procedure and NMR spectrum of **1**, additional TRIR data, methodology for data collection under molecular O_2, computational chemistry methods and further discussion (PDF)

The data supporting this research is openly available from the research data repository of the University of York at 10.15124/c0306cc5-6523-4889-a7c7-a6633d151526

■ AUTHOR INFORMATION

Corresponding Authors

Ian J. S. Fairlamb − *Department of Chemistry, University of York, York YO10 5DD, U.K.;* orcid.org/0000-0002-7555-2761; Email: ian.fairlamb@york.ac.uk

Jason M. Lynam − *Department of Chemistry, University of York, York YO10 5DD, U.K.;* orcid.org/0000-0003-0103-9479; Email: jason.lynam@york.ac.uk

Authors

Jonathan B. Eastwood − *Department of Chemistry, University of York, York YO10 5DD, U.K.;* orcid.org/0000-0001-5586-7697

Conor D. Rankine − *Department of Chemistry, University of York, York YO10 5DD, U.K.;* orcid.org/0000-0002-7104-847X

Thomas J. Burden − *Department of Chemistry, University of York, York YO10 5DD, U.K.;* orcid.org/0000-0001-9418-686X

Abigail Frith − *Department of Chemistry, University of York, York YO10 5DD, U.K.; School of Chemistry, Analytical & Biological Chemistry Research Facility, University College Cork, Cork T12 YN60, Ireland;* orcid.org/0009-0009-8770-787X

L. Anders Hammarback − *Department of Chemistry, University of York, York YO10 5DD, U.K.;* orcid.org/0000-0003-1336-6848

Barbara Procacci − *Department of Chemistry, University of York, York YO10 5DD, U.K.;* orcid.org/0000-0001-7044-0560

Daniel J. Shaw − *Department of Chemistry, University of York, York YO10 5DD, U.K.;* orcid.org/0000-0003-0090-2947

Benjamin R. O'Donoghue − *Department of Chemistry, University of York, York YO10 5DD, U.K.; School of Chemistry, Analytical & Biological Chemistry Research Facility, University College Cork, Cork T12 YN60, Ireland*

Ian P. Clark − *Central Laser Facility, Research Complex at Harwell, STFC, Rutherford Appleton Laboratory, Didcot OX11 0QX, U.K.;* orcid.org/0000-0002-0105-4743

Gabriel Karas − *Central Laser Facility, Research Complex at Harwell, STFC, Rutherford Appleton Laboratory, Didcot OX11 0QX, U.K.*

Partha Malakar − *Central Laser Facility, Research Complex at Harwell, STFC, Rutherford Appleton Laboratory, Didcot OX11 0QX, U.K.;* orcid.org/0000-0001-6874-7010

Gregory M. Greetham − *Central Laser Facility, Research Complex at Harwell, STFC, Rutherford Appleton Laboratory, Didcot OX11 0QX, U.K.;* orcid.org/0000-0002-1852-3403

Michael Towrie − *Central Laser Facility, Research Complex at Harwell, STFC, Rutherford Appleton Laboratory, Didcot OX11 0QX, U.K.;* orcid.org/0000-0002-1305-701X

Neil T. Hunt − *Department of Chemistry, University of York, York YO10 5DD, U.K.;* orcid.org/0000-0001-7400-5152

Gerard P. McGlacken − *School of Chemistry, Analytical & Biological Chemistry Research Facility, University College Cork, Cork T12 YN60, Ireland;* orcid.org/0000-0002-7821-0804

Complete contact information is available at: https://pubs.acs.org/10.1021/jacs.5c16761

Notes

The authors declare no competing financial interest.

■ ACKNOWLEDGMENTS

The authors are grateful to Syngenta, the EPSRC, and the Department of Chemistry at the University of York (iCASE studentship to L.A.H. EP/N509413/1, studentships for J.B.E. and T.J.B.) as well as the Royal Society of Chemistry (Research Enablement Grant to support J.B.E.), the EPSRC (grant number EP/W031914/1), and the Leverhulme Trust (RPG-2021-160, support for B.P.) for funding. The authors thank the STFC for program access to the ULTRA facility (grant number 1813). J.M.L. and I.J.S.F. are both supported by Royal Society Industry Fellowships (INF\R1\221057 and INF\R2\202122 respectively). Funding from Research Ireland (previously the Irish Research Council and Science Foundation Ireland (21/FFP-A/8784)) is also gratefully acknowledged. The authors are particularly grateful to Robin N. Perutz (York) for insightful comments about this study and its findings and to Andrew Orr-Ewing (Bristol) for highlighting the work on the photodissociation of thiophenols.

■ REFERENCES

(1) Schultz, D. M.; Yoon, T. P. Solar Synthesis: Prospects in Visible Light Photocatalysis. *Science* **2014**, *343*, 1239176.

(2) Prier, C. K.; Rankic, D. A.; MacMillan, D. W. C. Visible Light Photoredox Catalysis with Transition Metal Complexes: Applications in Organic Synthesis. *Chem. Rev.* **2013**, *113*, 5322−5363.

(3) Shaw, M. H.; Twilton, J.; MacMillan, D. W. C. Photoredox Catalysis in Organic Chemistry. *J. Org. Chem.* **2016**, *81*, 6898−6926.

(4) Marzo, L.; Pagire, S. K.; Reiser, O.; König, B. Visible-Light Photocatalysis: Does It Make a Difference in Organic Synthesis? *Angew. Chem., Int. Ed.* **2018**, *57*, 10034−10072.

(5) Hari, D. P.; König, B. Synthetic applications of eosin Y in photoredox catalysis. *Chem. Commun.* **2014**, *50*, 6688−6699.

(6) Dutta, S.; Erchinger, J. E.; Strieth-Kalthoff, F.; Kleinmans, R.; Glorius, F. Energy transfer photocatalysis: exciting modes of reactivity. *Chem. Soc. Rev.* **2024**, *53*, 1068−1089.

(7) Juliá, F.; Constantin, T.; Leonori, D. Applications of Halogen-Atom Transfer (XAT) for the Generation of Carbon Radicals in Synthetic Photochemistry and Photocatalysis. *Chem. Rev.* **2022**, *122*, 2292−2352.

(8) Jamatia, R.; Mondal, A.; Srimani, D. Visible-Light-Induced Manganese-Catalyzed Reactions: Present Approach and Future Prospects. *Adv. Synth. Catal.* **2021**, *363*, 2969−2995.

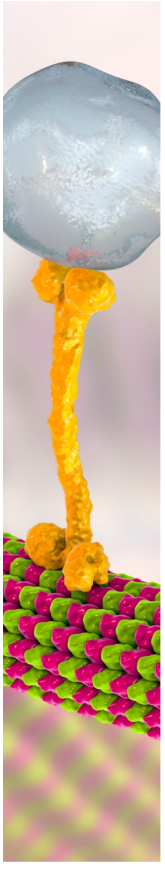
(9) Simpson, C. P.; Adebolu, O. I.; Kim, J. S.; Vasu, V.; Asandei, A. D. Metal and Ligand Effects of Photoactive Transition Metal Carbonyls in the Iodine Degenerative Transfer Controlled Radical Polymerization

and Block Copolymerization of Vinylidene Fluoride. *Macromolecules* **2015**, *48*, 6404−6420.
(10) Cernoch, P.; Petrova, S.; Cernochová, Z.; Kim, J. S.; Simpson, C. P.; Asandei, A. D. $Mn_2(CO)_{10}$-photomediated synthesis of poly(vinylidene fluoride)-*b*-poly(styrene sulfonate). *Eur. Polym. J.* **2015**, *68*, 460−470.
(11) Asandei, A. D.; Adebolu, O. I.; Simpson, C. P. Mild-Temperature $Mn_2(CO)_{10}$-Photomediated Controlled Radical Polymerization of Vinylidene Fluoride and Synthesis of Well-Defined Poly(vinylidene fluoride) Block Copolymers. *J. Am. Chem. Soc.* **2012**, *134*, 6080−6083.
(12) Wang, L.; Lear, J. M.; Rafferty, S. M.; Fosu, S. C.; Nagib, D. A. Ketyl radical reactivity via atom transfer catalysis. *Science* **2018**, *362*, 225−229.
(13) Rafferty, S. M.; Rutherford, J. E.; Zhang, L.; Wang, L.; Nagib, D. A. Cross-Selective Aza-Pinacol Coupling via Atom Transfer Catalysis. *J. Am. Chem. Soc.* **2021**, *143*, 5622−5628.
(14) Vivien, A.; Veyre, L.; Mirgalet, R.; Camp, C.; Thieuleux, C. $Mn_2(CO)_{10}$ and UV light: a promising combination for regioselective alkene hydrosilylation at low temperature. *Chem. Commun.* **2022**, *58*, 4091−4094.
(15) Laru, S.; Bhattacharjee, S.; Hajra, A. Visible-light-induced Mn(0)-catalyzed direct C-3 mono-, di- and perfluoroalkylation reactions of 2H-indazoles. *Chem. Commun.* **2022**, *58*, 13604−13607.
(16) Song, X. H.; Meng, S. S.; Zhang, H.; Jiang, Y.; Chan, A. S. C.; Zou, Y. Dibrominated addition and substitution of alkenes catalyzed by $Mn_2(CO)_{10}$. *Chem. Commun.* **2021**, *57*, 13385−13388.
(17) Schlichter, P.; Werlé, C. The Rise of Manganese-Catalyzed Reduction Reactions. *Synthesis* **2022**, *54*, 517−534.
(18) Liu, X.-G.; Dong, C.-S.; Li, F.; Zhang, B. Manganese-Mediated Direct Functionalization of Hantzsch Esters with Alkyl Iodides via an Aromatization−Dearomatization Strategy. *Org. Lett.* **2021**, *23*, 4002−4007.
(19) Ji, Y.-X.; Li, J.; Li, C.-M.; Qu, S.; Zhang, B. Manganese-Catalyzed N−F Bond Activation for Hydroamination and Carboamination of Alkenes. *Org. Lett.* **2021**, *23*, 207−212.
(20) Guo, Y.; Cao, Y.; Song, H.; Liu, Y.; Wang, Q. Photoredox relay-catalyzed gem-difluoroallylation of alkyl iodides. *Chem. Commun.* **2021**, *57*, 9768−9771.
(21) Dong, J.; Yuan, X.-A.; Yan, Z.; Mu, L.; Ma, J.; Zhu, C.; Xie, J. Manganese-catalysed divergent silylation of alkenes. *Nat. Chem.* **2021**, *13*, 182−190.
(22) Ji, Y.-X.; Wang, L.-J.; Guo, W.-S.; Bi, Q.; Zhang, B. Intermolecular Iodofluoroalkylation of Unactivated Alkynes and Alkenes Mediated by Manganese Catalysts. *Adv. Synth. Catal.* **2020**, *362*, 1131−1137.
(23) Weng, W.-Z.; Liang, H.; Liu, R.-Z.; Ji, Y.-X.; Zhang, B. Visible-Light-Promoted Manganese-Catalyzed Atom Transfer Radical Cyclization of Unactivated Alkyl Iodides. *Org. Lett.* **2019**, *21*, 5586−5590.
(24) Yang, X.; Wang, C. Dichotomy of Manganese Catalysis via Organometallic or Radical Mechanism: Stereodivergent Hydrosilylation of Alkynes. *Angew. Chem., Int. Ed.* **2018**, *57*, 923−928.
(25) Nuhant, P.; Oderinde, M. S.; Genovino, J.; Juneau, A.; Gagné, Y.; Allais, C.; Chinigo, G. M.; Choi, C.; Sach, N. W.; Bernier, L.; Fobian, Y. M.; Bundesmann, M. W.; Khunte, B.; Frenette, M.; Fadeyi, O. O. Visible-Light-Initiated Manganese Catalysis for C−H Alkylation of Heteroarenes: Applications and Mechanistic Studies. *Angew. Chem., Int. Ed.* **2017**, *56*, 15309−15313.
(26) Koumura, K.; Satoh, K.; Kamigaito, M. $Mn_2(CO)_{10}$-Induced Controlled/Living Radical Copolymerization of Vinyl Acetate and Methyl Acrylate: Spontaneous Formation of Block Copolymers Consisting of Gradient and Homopolymer Segments. *J. Polym. Sci., Polym. Chem.* **2009**, *47*, 1343−1353.
(27) Koumura, K.; Satoh, K.; Kamigaito, M. Manganese-Based Controlled/Living Radical Polymerization of Vinyl Acetate, Methyl Acrylate, and Styrene: Highly Active, Versatile, and Photoresponsive Systems. *Macromolecules* **2008**, *41*, 7359−7367.
(28) Liang, H.; Ji, Y. X.; Wang, R. H.; Zhang, Z. H.; Zhang, B. Visible-Light-Initiated Manganese-Catalyzed E-Selective Hydrosilylation and Hydrogermylation of Alkynes. *Org. Lett.* **2019**, *21*, 2750−2754.
(29) Goncharova, I. K.; Filatov, S. A.; Drozdov, A. P.; Tereshchenko, A. A.; Knyazev, P. A.; Guda, A. A.; Beletskaya, I. P.; Arzumanyan, A. V. White-Light initiated $Mn_2(CO)_{10}$/HFIP-Catalyzed anti-Markovnikov hydrosilylation of alkenes. *J. Catal.* **2024**, *429*, 115269.
(30) Koumura, K.; Satoh, K.; Kamigaito, M. $Mn_2(CO)_{10}$-Induced RAFT Polymerization of Vinyl Acetate, Methyl Acrylate, and Styrene. *Polym. J.* **2009**, *41*, 595−603.
(31) Liu, R. Z.; Li, J. X.; Sun, J.; Liu, X. G.; Qu, S. L.; Li, P.; Zhang, B. Generation and Reactivity of Amidyl Radicals: Manganese-Mediated Atom-Transfer Reaction. *Angew. Chem., Int. Ed.* **2020**, *59*, 4428−4433.
(32) Zhang, J. Z.; Harris, C. B. Photodissociation Dynamics of $Mn_2(CO)_{10}$ in Solution on Ultrafast Time Scales. *J. Chem. Phys.* **1991**, *95*, 4024−4032.
(33) Steinhurst, D. A.; Baronavski, A. P.; Owrutsky, J. C. Transient infrared spectroscopy of $Mn_2(CO)_{10}$ with 400 nm excitation. *Chem. Phys. Lett.* **2002**, *361*, 513−519.
(34) Cho, H.; Hong, K.; Strader, M. L.; Lee, J. H.; Schoenlein, R. W.; Huse, N.; Kim, T. K. Electronic and Molecular Structure of the Transient Radical Photocatalyst $Mn(CO)_5$ and Its Parent Compound $Mn_2(CO)_{10}$. *Inorg. Chem.* **2016**, *55*, 5895−5903.
(35) Turner, J. J.; George, M. W.; Poliakoff, M.; Perutz, R. N. Photochemistry of transition metal carbonyls. *Chem. Soc. Rev.* **2022**, *51*, 5300−5329.
(36) Li, C. M.; Dong, X. X.; Wang, Z.; Zhang, B. Visible light-initiated manganese-catalyzed hydrosulfonylation of alkenes. *Green Chem.* **2023**, *25*, 4122−4128.
(37) Han, J.; Han, J.; Chen, S.; Zhong, T.; He, Y. J.; Yang, X. L.; Wang, G. Q.; Zhu, C. J.; Xie, J. Photoinduced manganese-catalysed hydrofluorocarbofunctionalization of alkenes. *Nat. Synth.* **2022**, *1*, 475−486.
(38) Koizumi, H.; Tamaki, Y.; Kamogawa, K.; Nicaso, M.; Suzuki, Y.; Yamazaki, Y.; Takeda, H.; Ishitani, O. Development of a Highly Durable Photocatalytic CO Reduction Using a Mn-Complex Catalyst: Application of Selective Photosplitting of a Mn(0)-Mn(0) Bond. *J. Am. Chem. Soc.* **2025**, *147*, 6236−6248.
(39) Fairlamb, I. J. S.; Lynam, J. M. Unveiling Mechanistic Complexity in Manganese-Catalyzed C-H Bond Functionalization Using IR Spectroscopy Over 16 Orders of Magnitude in Time. *Acc. Chem. Res.* **2024**, *57*, 919−932.
(40) Eastwood, J. B.; Burden, T. J.; Hammarback, L. A.; Horbaczewskyj, C.; Tanner, T. F. N.; Clark, I. P.; Greetham, G.; Towrie, M.; Fairlamb, I. J. S.; Lynam, J. M. The importance of understanding (pre)catalyst activation in versatile C-H bond functionalisations catalysed by $[Mn_2(CO)_{10}]$. *Chem. Sci.* **2024**, *15*, 9183−9191.
(41) Eastwood, J. B.; Hammarback, L. A.; Burden, T. J.; Clark, I. P.; Towrie, M.; Robinson, A.; Fairlamb, I. J. S.; Lynam, J. M. Understanding Precatalyst Activation and Speciation in Manganese-Catalyzed C-H Bond Functionalization Reactions. *Organometallics* **2023**, *42*, 1766−1773.
(42) Burden, T. J.; Fernandez, K. P. R.; Kagoro, M.; Eastwood, J. B.; Tanner, T. F. N.; Whitwood, A. C.; Clark, I. P.; Towrie, M.; Krieger, J. P.; Lynam, J. M.; Fairlamb, I. J. S. Coumarin C-H Functionalization by Mn(I) Carbonyls: Mechanistic Insight by Ultra-Fast IR Spectroscopic Analysis. *Chem. Eur J.* **2023**, *29*, No. e202203038.
(43) Hammarback, L. A.; Eastwood, J. B.; Burden, T. J.; Pearce, C. J.; Clark, I. P.; Towrie, M.; Robinson, A.; Fairlamb, I. J. S.; Lynam, J. M. A comprehensive understanding of carbon-carbon bond formation by alkyne migratory insertion into manganacycles. *Chem. Sci.* **2022**, *13*, 9902−9913.
(44) Hammarback, L. A.; Bishop, A. L.; Jordan, C.; Athavan, G.; Eastwood, J. B.; Burden, T. J.; Bray, J. T. W.; Clarke, F.; Robinson, A.; Krieger, J. P.; Whitwood, A.; Clark, I. P.; Towrie, M.; Lynam, J. M.; Fairlamb, I. J. S. Manganese-Mediated C-H Bond Activation of Fluorinated Aromatics and the ortho-Fluorine Effect: Kinetic Analysis by Infrared Spectroscopic Analysis and Time-Resolved Methods. *ACS Catal.* **2022**, *12*, 1532−1544.
(45) Hammarback, L. A.; Aucott, B. J.; Bray, J. T. W.; Clark, I. P.; Towrie, M.; Robinson, A.; Fairlamb, I. J. S.; Lynam, J. M. Direct

Observation of the Microscopic Reverse of the Ubiquitous Concerted Metalation Deprotonation Step in C-H Bond Activation Catalysis. *J. Am. Chem. Soc.* **2021**, *143*, 1356−1364.
(46) Firth, J. D.; Hammarback, L. A.; Burden, T. J.; Eastwood, J. B.; Donald, J. R.; Horbaczewskyj, C. S.; McRobie, M. T.; Tramaseur, A.; Clark, I. P.; Towrie, M.; Robinson, A.; Krieger, J. P.; Lynam, J. M.; Fairlamb, I. J. S. Light- and Manganese-Initiated Borylation of Aryl Diazonium Salts: Mechanistic Insight on the Ultrafast Time-Scale Revealed by Time-Resolved Spectroscopic Analysis. *Chem. Eur J.* **2021**, *27*, 3979−3985.
(47) Eastwood, J. B.; Hammarback, L. A.; McRobie, M. T.; Clark, I. P.; Towrie, M.; Fairlamb, I. J. S.; Lynam, J. M. Time-resolved infra-red spectroscopy reveals competitive water and dinitrogen coordination to a manganese(I) carbonyl complex. *Dalton Trans.* **2020**, *49*, 5463−5470.
(48) Hammarback, L. A.; Robinson, A.; Lynam, J. M.; Fairlamb, I. J. S. Mechanistic Insight into Catalytic Redox-Neutral C-H Bond Activation Involving Manganese(I) Carbonyls: Catalyst Activation, Turnover, and Deactivation Pathways Reveal an Intricate Network of Steps. *J. Am. Chem. Soc.* **2019**, *141*, 2316−2328.
(49) Hammarback, L. A.; Robinson, A.; Lynam, J. M.; Fairlamb, I. J. S. Delineating the critical role of acid additives in Mn-catalysed C-H bond functionalisation processes. *Chem. Commun.* **2019**, *55*, 3211−3214.
(50) Aucott, B. J.; Eastwood, J. B.; Anders Hammarback, L.; Clark, I. P.; Sazanovich, I. V.; Towrie, M.; Fairlamb, I. J. S.; Lynam, J. M. Insight into the mechanism of CO-release from trypto-CORM using ultra-fast spectroscopy and computational chemistry. *Dalton Trans.* **2019**, *48*, 16426−16436.
(51) Aucott, B. J.; Duhme-Klair, A. K.; Moulton, B. E.; Clark, I. P.; Sazanovich, I. V.; Towrie, M.; Hammarback, L. A.; Fairlamb, I. J. S.; Lynam, J. M. Manganese Carbonyl Compounds Reveal Ultrafast Metal-Solvent Interactions. *Organometallics* **2019**, *38*, 2391−2401.
(52) Hammarback, L. A.; Clark, I. P.; Sazanovich, I. V.; Towrie, M.; Robinson, A.; Clarke, F.; Meyer, S.; Fairlamb, I. J. S.; Lynam, J. M. Mapping out the key carbon-carbon bond-forming steps in Mn-catalysed C-H functionalization. *Nat. Catal.* **2018**, *1*, 830−840.
(53) Bianchi, R.; Gervasio, G.; Marabello, D. Experimental electron density analysis of $Mn_2(CO)_{10}$: Metal-metal and metal-ligand bond characterization. *Inorg. Chem.* **2000**, *39*, 2360−2366.
(54) Levine, D. S.; Head-Gordon, M. Energy decomposition analysis of single bonds within Kohn-Sham density functional theory. *Proc. Natl. Acad. Sci.* **2017**, *114*, 12649−12656.
(55) Joy, J.; Danovich, D.; Kaupp, M.; Shaik, S. Covalent vs Charge-Shift Nature of the Metal-Metal Bond in Transition Metal Complexes: A Unified Understanding. *J. Am. Chem. Soc.* **2020**, *142*, 12277−12287.
(56) Kaupp, M. The role of radial nodes of atomic orbitals for chemical bonding and the periodic table. *J. Comput. Chem.* **2007**, *28*, 320−325.
(57) Martin, M.; Rees, B.; Mitschler, A. Bonding in a Binuclear Metal-Carbonyl - Experimental Charge-Density in $Mn_2(CO)_{10}$. *Acta. Crystallogr. B* **1982**, *38*, 6−15.
(58) Dahl, L. F.; Rundle, R. E. Crystal Structure of Dimanganese Decacarbonyl, $Mn_2(CO)_{10}$. *Acta Crystallogr.* **1963**, *16*, 419−426.
(59) Almenningen, A.; Jacobsen, G. G.; Seip, H. M.; Lindblad, C. G.; Lindberg, A. A.; Jansen, G.; Lamm, B.; Samuelsson, B. On Molecular Structure of Dimanganese Decacarbonyl $Mn_2(CO)_{10}$. *Acta Chem. Scand.* **1969**, *23*, 685−686.
(60) Yan, C.; Radzhabov, M. R.; Chang, T. Y.; Chen, Y. S.; Mankad, N. P. Comprehensive Re-examination of Intermetallic Charge Density for the Metal Carbonyl Dimers $Mn_2(CO)_{10}$ and $[(\eta^5\text{-}C_5H_5)Fe(CO)_2]_2$. *Inorg. Chem.* **2025**, *64*, 4514−4523.
(61) Sellin, M.; Koger, H.; Engesser, T. A.; Grunenberg, J.; Krossing, I. Isolation and Characterization of $[MnFe(CO)_{10}]^+$: The Missing Link in the 3d Dimetal Decacarbonyl Series. *Chem. Eur J.* **2025**, *31*, No. e202500489.
(62) Berg, W. R.; Reimann, M.; Sievers, R.; Rupf, S. M.; Schlögl, J.; Weisser, K.; Krause, K. B.; Limberg, C.; Kaupp, M.; Malischewski, M. Solvent-Dependent Reactivity of $Fe(CO)_5$ under Superacidic and Oxidative Conditions. *J. Am. Chem. Soc.* **2025**, *147*, 3039−3046.
(63) Greetham, G. M.; Sole, D.; Clark, I. P.; Parker, A. W.; Pollard, M. R.; Towrie, M. Time-resolved multiple probe spectroscopy. *Rev. Sci. Instrum.* **2012**, *83*, 103107.
(64) Greetham, G. M.; Donaldson, P. M.; Nation, C.; Sazanovich, I. V.; Clark, I. P.; Shaw, D. J.; Parker, A. W.; Towrie, M. A 100 kHz Time-Resolved Multiple-Probe Femtosecond to Second Infrared Absorption Spectrometer. *Appl. Spectrosc.* **2016**, *70*, 645−653.
(65) Rothberg, L. J.; Cooper, N. J.; Peters, K. S.; Vaida, V. Picosecond Dynamics of Solution-Phase Photofragmentation of $[Mn_2(CO)_{10}]$. *J. Am. Chem. Soc.* **1982**, *104*, 3536−3537.
(66) Parker, D. J.; Stiddard, M. H. Vibrational and Electronic Spectra of Transition-Metal Carbonyl Complexes. Part I. Infrared Spectra of Decacarbonyldimanganese and Its Derivatives. *J. Chem. Soc. A* **1966**, 695−699.
(67) Church, S. P.; Poliakoff, M.; Timney, J. A.; Turner, J. J. Synthesis and Characterization of the Pentacarbonylmanganese(0) Radical, $Mn(CO)_5$, in Low-Temperature Matrices. *J. Am. Chem. Soc.* **1981**, *103*, 7515−7520.
(68) Baiz, C. R.; McRobbie, P. L.; Preketes, N. K.; Kubarych, K. J.; Geva, E. Two-Dimensional Infrared Spectroscopy of Dimanganese Decacarbonyl and Its Photoproducts: An Ab Initio Study. *J. Phys. Chem. A* **2009**, *113*, 9617−9623.
(69) Farmer, A. L.; Procacci, B.; Shaw, D. J.; Gurung, S.; Fairlamb, I. J. S.; Lynam, J. M.; Hunt, N. T. Ultrafast vibrational spectroscopic analysis of the ubiquitous precatalyst $[Mn_2(CO)_{10}]$ in different solvents. *J. Chem. Phys.* **2025**, *162*, 174302.
(70) Irradiation of $[Mn_2(CO)_{10}]$ at 400 nm does result in a small amount of CO-photodissociation (q.v.) − geminate recombination of CO and $[Mn_2(CO)_9]$ will also result in vibrationally excited $[Mn_2(CO)_{10}]$. Analysis of the recovery of the ground state bleach on a ps time scale that arises from the cooling of hot $[Mn_2(CO)_{10}]$ reveals that ca. 76% of the light-generated photoproducts undergo geminate recombination through either pathway.
(71) Arrivo, S. M.; Dougherty, T. P.; Grubbs, W. T.; Heilweil, E. J. Ultrafast Infrared-Spectroscopy of Vibrational CO-Stretch up-Pumping and Relaxation Dynamics of $W(CO)_6$. *Chem. Phys. Lett.* **1995**, *235*, 247−254.
(72) Strasfeld, D. B.; Shim, S. H.; Zanni, M. T. Controlling vibrational excitation with shaped mid-IR pulses. *Phys. Rev. Lett.* **2007**, *99*, 038102.
(73) Reed, Z. D.; Duncan, M. A. Infrared spectroscopy and structures of manganese carbonyl cations, $Mn(CO)_n^+$ (n = 1−9). *J. Am. Soc. Mass Spectrom.* **2010**, *21*, 739−749.
(74) Pribula, C. D.; Brown, T. L. Metal-Ion Interactions with $Mn(CO)_5^-$ in Ether Solutions. *J. Organomet. Chem.* **1974**, *71*, 415−425.
(75) Darensbourg, M. Y.; Darensbourg, D. J.; Burns, D.; Drew, D. A. Infrared, Conductance, and Kinetic Evidence for Alkali-Metal Ion Interactions with Derivatives of Manganese Carbonylates. *J. Am. Chem. Soc.* **1976**, *98*, 3127−3136.
(76) Owrutsky, J. C.; Baronavski, A. P. Ultrafast infrared study of the ultraviolet photodissociation of $Mn_2(CO)_{10}$. *J. Chem. Phys.* **1996**, *105*, 9864−9873.
(77) Church, S. P.; Hermann, H.; Grevels, F. W.; Schaffner, K. The Primary Photoproducts of $Mn_2(CO)_{10}$ - Direct I.R. Observation and Decay Kinetics of $Mn(CO)_5$ and $Mn_2(CO)_9$ in Hydrocarbon Solution at Room-Temperature. *J. Chem. Soc, Chem. Commun.* **1984**, 785−786.
(78) Braden, D. A.; Parrack, E. E.; Tyler, D. R. Solvent cage effects. I. Effect of radical mass and size on radical cage pair recombination efficiency. II. Is geminate recombination of polar radicals sensitive to solvent polarity? *Coord. Chem. Rev.* **2001**, *211*, 279−294.
(79) Braden, D. A.; Parrack, E. E.; Tyler, D. R. Photochemical studies as a function of solvent viscosity.: A new photochemical pathway in the reaction of $(\eta^5\text{-}C_5H_4Me)_2Mo_2(CO)_6$ with CCl_4. *Photochem. Photobiol. Sci.* **2002**, *1*, 418−420.
(80) Harris, J. D.; Oelkers, A. B.; Tyler, D. R. The Solvent Cage Effect: Is There a Spin Barrier to Recombination of Transition Metal Radicals? *J. Am. Chem. Soc.* **2007**, *129*, 6255−6262.
(81) Barry, J. T.; Berg, D. J.; Tyler, D. R. Radical Cage Effects: Comparison of Solvent Bulk Viscosity and Microviscosity in Predicting

https://doi.org/10.1021/jacs.5c16761
J. Am. Chem. Soc. 2026, 148, 15450−15462

the Recombination Efficiencies of Radical Cage Pairs. *J. Am. Chem. Soc.* **2016**, *138*, 9389−9392.
(82) Barry, J. T.; Berg, D. J.; Tyler, D. R. Radical Cage Effects: The Prediction of Radical Cage Pair Recombination Efficiencies Using Microviscosity Across a Range of Solvent Types. *J. Am. Chem. Soc.* **2017**, *139*, 14399−14405.
(83) Goodman, J. L.; Peters, K. S.; Vaida, V. The Determination of the Mn-Mn Bond Strength in $Mn_2(CO)_{10}$ Using Pulsed Time-Resolved Photoacoustic Calorimetry. *Organometallics* **1986**, *5*, 815−816.
(84) Bidinost, D. R.; McIntyre, N. S. Mass Spectrometric Study of Thermal Decomposition of Dimanganese Decacarbonyl and Dicobalt Octacarbonyl. *Can. J. Chem.* **1970**, *48*, 593−597.
(85) Svec, H. J.; Junk, G. A. Energetics of Ionization and Dissociation of $Mn_2(CO)_{10}$, $Re_2(CO)_{10}$, and $ReMn(CO)_{10}$. *J. Am. Chem. Soc.* **1967**, *89*, 2836−2840.
(86) Folga, E.; Ziegler, T. A Density-Functional Study on the Strength of the Metal Bonds in $Co_2(CO)_8$ and $Mn_2(CO)_{10}$ and the Metal Hydrogen and Metal-Carbon Bonds in R-$Mn(CO)_5$ and R-$Co(CO)_4$. *J. Am. Chem. Soc.* **1993**, *115*, 5169−5176.
(87) Simoes, J. A. M.; Schultz, J. C.; Beauchamp, J. L. Ion-Cyclotron Resonance and Photoelectron Studies of the Ionization Energetics and Thermochemical Properties of $Mn(CO)_5$(Benzyl) - Implications for the Manganese Manganese Bond Strength in $Mn_2(CO)_{10}$. *Organometallics* **1985**, *4*, 1238−1242.
(88) Marcomini, A.; Poe, A. Kinetics of the Scrambling Reaction between Dimanganese and Dirhenium Decacarbonyl. *J. Am. Chem. Soc.* **1983**, *105*, 6952−6958.
(89) Smith, G. P. Gas-Phase 1st Bond-Dissociation Energies in Transition-Metal Carbonyls. *Polyhedron* **1988**, *7*, 1605−1608.
(90) Ashfold, M. N. R.; Devine, A. L.; Dixon, R. N.; King, G. A.; Nix, M. G. D.; Oliver, T. A. A. Exploring nuclear motion through conical intersections in the UV photodissociation of phenols and thiophenol. *Proc. Natl. Acad. Sci.* **2008**, *105*, 12701−12706.
(91) Zhang, Y. Y.; Oliver, T. A. A.; Das, S.; Roy, A.; Ashfold, M. N. R.; Bradforth, S. E. Exploring the Energy Disposal Immediately After Bond-Breaking in Solution: The Wavelength-Dependent Excited State Dissociation Pathways of para-Methylthiophenol. *J. Phys. Chem. A* **2013**, *117*, 12125−12137.
(92) Oliver, T. A. A.; King, G. A.; Tew, D. P.; Dixon, R. N.; Ashfold, M. N. R. Controlling Electronic Product Branching at Conical Intersections in the UV Photolysis of para-Substituted Thiophenols. *J. Phys. Chem. A* **2012**, *116*, 12444−12459.
(93) Drew, D.; Darensbourg, D. J.; Darensbourg, M. Y. Synthesis, spectral properties, and reactions of manganese and rhenium pentacarbonyl phosphine and phosphite cation derivatives and related complexes. *Inorg. Chem.* **1975**, *14*, 1579−1584.
(94) Hyam, I. J.; Lippincott, E. R. A Vibrational Assignment for Manganese Carbonyl Halides. *Spectrochim. Acta, Part A* **1969**, *25*, 1845−1854.
(95) Orgel, L. E. The Infrared Spectra of Substituted Metal Carbonyls. *Inorg. Chem.* **1962**, *1*, 25−29.
(96) Fieldhouse, S. A.; Fullam, B. W.; Neilson, G. W.; Symons, M. C. R. Reaction of Metal-Carbonyls with Oxygen. *J. Chem. Soc., Dalton Trans.* **1974**, 567−569.
(97) Hudson, A.; Lappert, M. F.; Nicholson, B. K. Reassignment to a Manganese(II) Species of an ESR-Spectrum Attributed to $Mn(CO)_5$. *J. Organomet. Chem.* **1975**, *92*, C11−C14.
(98) Kwan, C. L.; Kochi, J. K. Esr-Spectrum of Manganese Species in Photolysis of $Mn_2(CO)_{10}$ in Solution. *J. Organomet. Chem.* **1975**, *101*, C9−C13.
(99) Kumar Jha, R.; Rohilla, K.; Jain, S.; Parganiha, D.; Kumar, S. Blue-Light Irradiated Mn(0)-Catalyzed Hydroxylation and C(sp^3)-H Functionalization of Unactivated Alkanes with C(sp^2)-H Bonds of Quinones for Alkylated Hydroxy Quinones and Parvaquone. *Chem. Eur J.* **2024**, *30*, No. e202303537.
(100) Caution: mixtures of hydrocarbons and oxygen are potentially explosive. See the Supporting Information of the experimental details used to mitigate this risk
(101) Battino, R.; Rettich, T. R.; Tominaga, T. The Solubility of Oxygen and Ozone in Liquids. *J. Phys. Chem. Ref. Data* **1983**, *12*, 163−178.
(102) Meyer, T. J.; Caspar, J. V. Photochemistry of Metal Metal Bonds. *Chem. Rev.* **1985**, *85*, 187−218.
(103) Hepp, A. F.; Wrighton, M. S. Relative Importance of Metal Metal Bond Scission and Loss of Carbon-Monoxide from Photo-Excited Dimanganese Decacarbonyl - Spectroscopic Detection of a Coordinatively Unsaturated, Co-Bridged Dinuclear Species in Low-Temperature Alkane Matrices. *J. Am. Chem. Soc.* **1983**, *105*, 5934−5935.
(104) Grevels, F. W.; Jacke, J.; Seevogel, K. Dynamics of Metal-Carbonyls on the Infrared Time Scale - Coalescence of CO Stretching Vibrational Bands. *J. Mol. Struct.* **1988**, *174*, 107−112.
(105) We are grateful to an anonomous reviewer for highlighting this possibility.
(106) Church, S. P.; Grevels, F. W.; Hermann, H.; Schaffner, K. Fast Infrared Detection of $Cr(CO)_5N_2$ in Room-Temperature Solution. *Inorg. Chem.* **1984**, *23*, 3830−3833.
(107) Frogley, B. J.; Hill, A. F.; Onagi, H.; Watson, L. J. Organometallic flow chemistry: solvento complexes. *Dalton Trans.* **2022**, *51*, 17354−17360.


CAS BIOFINDER DISCOVERY PLATFORM™
BRIDGE BIOLOGY AND CHEMISTRY FOR FASTER ANSWERS
Analyze target relationships, compound effects, and disease pathways
Explore the platform
CAS
A division of the American Chemical Society

https://doi.org/10.1021/jacs.5c16761
J. Am. Chem. Soc. 2026, 148, 15450−15462